Cellulose (2022) 29:4001–4019
https://doi.org/10.1007/s10570-022-04519-4

ORIGINAL RESEARCH

Copper ion-imprinted bacterial cellulose for selectively removing heavy metal ions from aqueous solution

Kang Xiaorui · Zhu Cong · Xiong Pin · Du Zhanwen · Cai Zhijiang

Received: 9 September 2021 / Accepted: 2 March 2022 / Published online: 18 March 2022

Abstract Novel surface copper ion-imprinted bacterial cellulose nanofiber nonwoven adsorbent was fabricated via surface ion-imprinting technique combined with electrospinning technology for highly selective adsorption of copper ions in aqueous solutions. The as-prepared nanofiber nonwoven adsorbent was characterized by scanning electron microscopy, specific surface area, Fourier transform infrared spectroscopy and energy dispersive X-ray, respectively. The adsorption capacity and recognition selectivity performance towards copper ions were investigated by batch experiments. The experimental data indicate that the ion-imprinted nanofiber nonwoven adsorbent presents excellent adsorption ability and high recognition selectivity towards copper ions in binary systems using zinc, nickel, lead and cadmium as competitive ions. The maximum copper ion adsorption capacity is determined to be 152.2 mg/g at 298 K, which is higher than that of the other imprinted adsorbents. The selectivity coefficients for copper ion adsorption in binary metal ion solution of copper/zinc, copper/nickel, copper/lead and copper/cadmium reach up to 47, 101, and 162, respectively. As illustrated by Scatchard models, the specific recognition site with high copper ion affinity should be a key factor affecting selective adsorption. In addition, the nanofiber nonwoven adsorbent exhibits good anti-interference ability and reusability. The nanofiber nonwoven adsorbent can be reused at least ten cycles with only 7.9% reduction in adsorption capacity. Therefore, the prepared copper ion-imprinted nanofiber nonwoven can be an effective adsorbent for separation or enrichment of copper ions for water treatment applications.

K. Xiaorui · Z. Cong · X. Pin · D. Zhanwen · C. Zhijiang (✉)
State Key Laboratory of Separation Membranes and Membrane Processes, School of Textiles Science and Engineering, Tiangong University, No 399 BingShuiXi Street, XiQing District, Tianjin 300387, China
e-mail: caizhijiang@hotmail.com

Graphical abstract

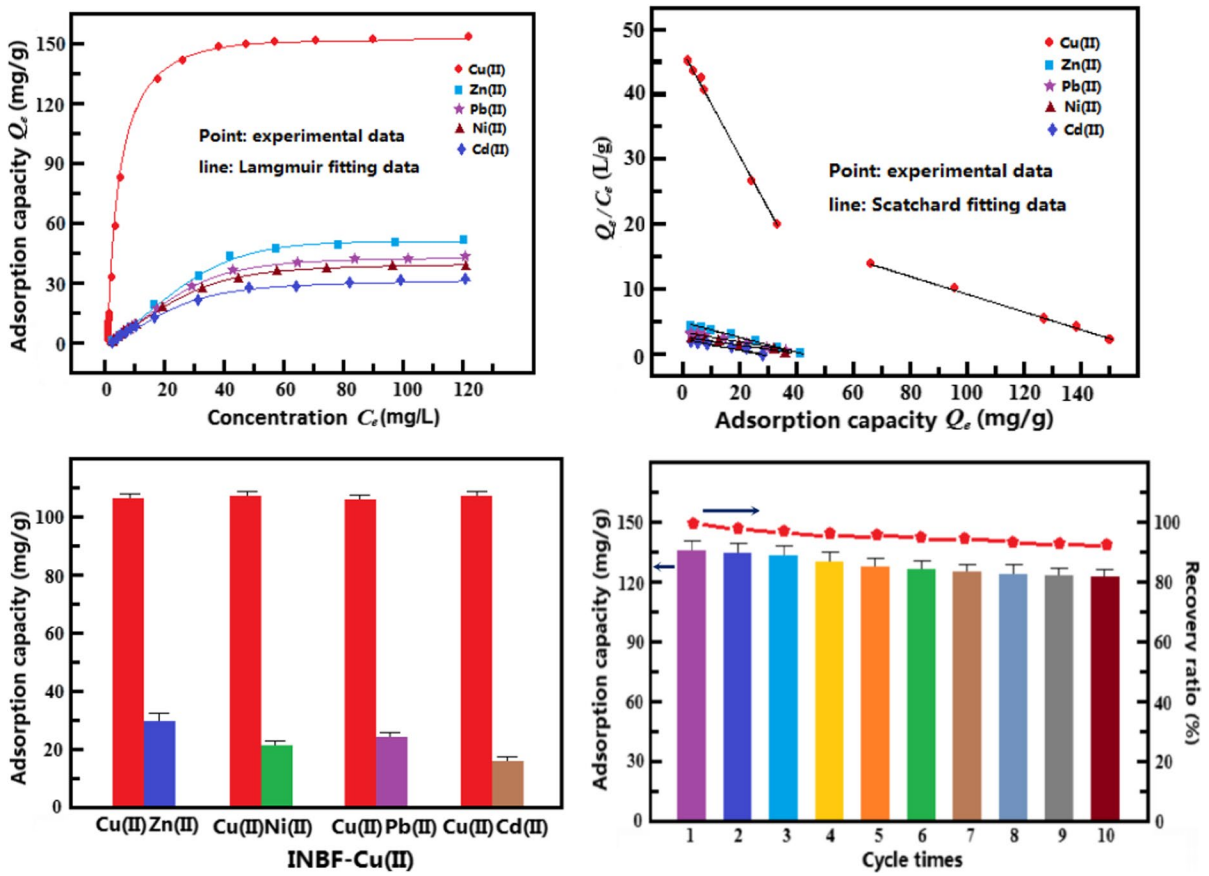

Keywords Ion-imprinting · Electrospinning · Nonwoven adsorbent · Adsorption · Selectivity

Introduction

Recently, water pollution has become one of the most significant environment problems due to rapid development of global industrialization. Inorganics (e.g. heavy metal ions) and organics (textile dyes) are major pollutants. These pollutants can get into the food chains by accumulation in living organisms, which might affect the environment as well as human health since they are toxic and cannot be degraded into non-toxic material unless they can be metabolized in time (Mahmoodi et al. 2007; Xu et al. 2018a, b; Kashefi et al. 2019). Thus, treatment of waste-water is an important research topic. By now, various methods including precipitation (Chen et al. 2018), coagulation (Kim et al. 2020), filtration (Nasrollahi et al. 2019; Skoczko et al. 2018), flocculation (Süreyya et al. 2002), ion exchange (Bashir et al. 2019), electrolysis (Bhagat et al. 2020), ultrasound-assisted synthesis (Abdi et al. 2017), photocatalytic (Mahmoodi 2014) and adsorption (Xu et al. 2018a, b) have been applied to remove heavy metal ions and dyes from aqueous solution. Among these methods, adsorption is most widely used owing to its easy operation, low cost, good reusability and high efficiency (Ngah et al. 2011). However, most adsorbents have disadvantages in selective recognition and adsorption.

Surface ion-imprinting method (SIIM) is a novel and effective technique to prepare adsorbents with high selectivity based on ion recognition-adsorption mechanism (He et al. 2018; Monier et al. 2013; Erol

et al. 2017). This technique involves support materials that selectively bind with the template ions on the surface layer. After removing the template ions, the binding sites are exposed and have positions with similar shape, size, and chemistry to target ions. As a result, surface ion-imprinting adsorbents (SIIA) present remarkable affinity and high selectivity towards target ions and can be applied to detection, adsorption, purification and environmental protection (Zhang et al. 2007, 2010; Bakhshpour et al. 2017). SIIA can be prepared by bulk polymerization (Wang et al. 2019a, b), suspension polymerization (Hoai et al. 2010), precipitation polymerization (Roushani et al. 2015; Pang et al. 2011), sol–gel process (Ren et al. 2018; Cai et al. 2014) and other methods (Zhu et al. 2017; Peng et al. 2015; Janmohammadi et al. 2018). For instance, Mishra and Verma (2017) reported a Pb(II) ions-imprinted polymeric beads by surface ion imprinting technique using suspension polymerization for Pb(II) removal from waste-water. The maximum adsorption capacity of Pb(II) was up to 47 mg/g with high selectivity coefficients.

Nowadays, electrospinning technology has been extensively investigated to fabricate nanofiber materials applied in the fields like tissue engineering, drug release systems, sensors, filtration and adsorption (Yu et al. 2018; Tripathy et al. 2019; Zhang et al. 2019; Mousavi et al. 2018; Wu et al. 2018). Compared with particle adsorbents, nanofiber adsorbents possess characteristics of good flexibility, large specific surface areas, high porosity, small pore size with interconnected structure and short transit distance. Furthermore, they can be fabricated into different shapes like nanofibers, membranes and nonwoven fabrics (Quan et al. 2018; Miao et al. 2013; Jiajia et al. 2020). It might be interesting to fabricate ion-imprinted nanofiber nonwoven fabric adsorbents by SIIM for selective removal of heavy metal ions in aqueous solution.

Environmentally friendly polymers based on green molecules such as chitosan and cellulose have been recommended for water treatment applications since they contain large mount of functional groups like amino, hydroxyl, carboxyl, etc. which can be effective to combine with heavy metal ions (Davarpanah et al. 2009; Wang, et al. 2019a, b; Zhao et al. 2019; Hong et al. 2018). Bacterial cellulose (BC) is one kind of environmentally friendly polymers, which has been bio-synthesized in large scale and commercially used in industrial applications. BC has many advantages in properties like high crystallinity, excellent mechanical properties, good hydrophilicity and biodegradability (Zhijiang et al. 2019; Hou et al. 2018). Since BC has high content of hydroxyl groups along molecular chains, it has been investigated as adsorbent for metal ions removal from aqueous solution. For example, BC/Graphene oxide hybrids (Fang et al. 2016), BC/attapulgite magnetic composites (Chen et al. 2019) and BC/Fe_3O_4 nanocomposites (Zhu et al. 2011) have been reported for Cu(II), Cd(II) and Pb(II) ions adsorption. However, these adsorbents show low ions selectivity. Recently, molecularly imprinted composite BC nanofibers for antibiotic release (Emel et al. 2019) and metal-ions imprinted thermo-responsive BC derivatives for Cu(II) adsorption (Li et al. 2019) have been illustrated by in-situ polymerization using molecule and metal ion as template.

In the present work, a novel surface Cu(II) ion-imprinted BC based nanofiber nonwoven fabric (IBCN-Cu) adsorbent was developed by two-step process combined with electrospinning technique and SIIM. The novelty of this research lies in that the BC based nanofibrous structure can provide large specific surface areas and large amount of hydroxyl functional groups favourable of metal ions adsorption and well-designed ion-imprinted recognition sites with coordination geometry matching with Cu(II) ions in charge, size, shape, coordination number and spatial arrangement of hydroxyl groups can remarkably improve recognition selectivity towards Cu(II) ions with excellent anti-interference ability. The as-obtained IBCN-Cu adsorbents were characterized with their physico-chemical characteristics by scanning electron microscopy (SEM), BET surface area, Fourier transform infrared spectroscopy (FTIR) and energy dispersive X-ray (EDX). The effects of various adsorption conditions such as solution concentration, solution pH, and competitive metal ions on IBCN-Cu adsorption behavior were investigated. The selectivity of Cu(II) binding onto IBCN-Cu was investigated to study the selective adsorption. The adsorption isotherm and kinetics were analyzed on the IBCN-Cu to explore the mechanism of selective separation. The adsorption capacity and selectivity coefficients of the prepared IBCN-Cu in this work was also compared with other Cu(II)-imprinted adsorbents reported in literature.

Experimental

Materials

Bacterial cellulose produced by Gluconacetobacter xylinum with molecular weight about 6.3×10^5 g/mol were kindly supplied Tianjin GreenBio Materials Co., Ltd. N,N-Dimethylacetamide (DMAc), ethanol, HCl (36 − 38 wt%), NaOH (purity > 96%) and glutaraldehyde were purchased from Sinopharm Chemical Reagent Co., Ltd (Beijing, China). Copper nitrate ($Cu(NO_3)_2$), lead nitrate ($Pb(NO_3)_2$), nickel nitrate ($Ni(NO_3)_2$), and cadmium nitrate ($Cd(NO_3)_2$) were purchased from Sinopharm Chemical Reagent Beijing Co., Ltd. All chemical reagents of the highest purity available were used as received without further treatment. Deionized water was used in all the experiments and prepared by our lab.

Instruments

The ion concentration in the aqueous solution was determined by inductively coupled plasma mass spectrometry (ICPMS-700, Perkin Elmer). The pH value of the aqueous solution was measured by pH meter (HI221, Hanna). The surface morphology of the samples were observed by scanning electron microscope (SEM, Hitachi S-4200). The chemical structure changes of the samples was monitored by Fourier transform infrared spectroscopy (FTIR2000, Perkin Elmer). The specific surface area of the samples was analyzed by Brunauer-Emmet-Teller (BET) method using surface area analyzer (BET, Sorptomatic-1990). The surface metal ion distribution was detected by energy dispersive X-ray (EDX, Oxford Inc., Germany).

Preparation of Cu(II) ion-imprinted BC based nanofiber nonwoven fabric adsorbent (IBCN-Cu)

IBCN-Cu was fabricated by two-step process combined with electrospinning technique and SIIM. For the first step, BC was dissolved in DMAc at 90 °C for 12 h to prepare 5 wt% BC spinning solution by continuously stir. The BC nanofiber nonwoven fabric was prepared by electrospinning technique under the following parameters: 25 kV for applied voltage, 1.0 mL/h for exclusion speed, 22 cm for collecting distance, 25 °C for temperature and 35% for relative humidity. After electrospinning process, the BC nanofiber nonwoven fabric was dried under vacuum at room temperature to remove solvent completely. The sample was labeled as BNF and used for further preparation. For the second step, Cu(II) ions were imprinted onto BNF by SIIM. 0.2 g BC nanofiber nonwoven fabric was immersed in 50 mL of 400 mg/L Cu(II) aqueous solution at pH 5.0 for 4 h. Then, the nonwoven fabric was washed using moving water for 1 h to remove redundant Cu(II) ions on the nonwoven fabric. After that, the nonwoven fabric was crosslinked by 3 wt% glutaraldehyde aqueous solution at room temperature for 4 h. Finally, the nonwoven fabric was washed by HCl (1 mol/L) to remove the Cu(II) template ions until no Cu(II) ion was tested by ICP in the eluent. After washing by water to neutrality and drying under vacuum overnight, the Cu(II) ion surface imprinted BC based nanofiber nonwoven fabric was obtained and labeled as IBCN-Cu.

Adsorption study

All adsorption experiments were carried out by batch process using a vapour-bathing vibrator at certain temperature (298, 308 and 318 K, respectively) in 250 mL beakers and conducted in triplicate. Briefly, 0.1 g IBCN-Cu nonwoven adsorbent (M, adsorbent mass, g) was immersed into metal ion stock solutions of 150 mL (V, solution volume, L) with various initial concentration ($C_{i,}$ mg/L) for 4 h to achieve adsorption equilibration completely. Adsorption capacity at equilibrium (Q_e, mg/g) and time t (Q_t, mg/g) can be determined by the amount of metal ions adsorbed on unit mass of adsorbent using the following equations.

$$Q_e = \frac{(C_i - C_e)\times V}{M} \tag{1}$$

$$Q_t = \frac{(C_i - C_t)\times V}{M} \tag{2}$$

where C_e and C_t (mg/L) represent ion concentration after adsorption and at time t, respectively.

The effect of solution pH value, adsorption time and initial solution concentration on the adsorption capacity of the nanofiber nonwoven fabric adsorbent were investigated systematically.

Selective adsorption

The selectivity of the IBCN-Cu adsorbent for Cu(II) ions was evaluated in the presence of the competitive metal ions. The selective adsorption experiments were performed in the binary mixed solutions of Cu(II)/Zn(II), Cu(II)/Ni(II), Cu(II)/Pb(II), Cu(II)/Cd(II) with each ion initial concentration of 20 mg/L at a constant pH of 5.0 and at 298 K. The selective adsorption performance of the IBCN-Cu adsorbent for Cu(II) ions can be determined in term of adsorptive distribution coefficients (K_{ad}), adsorptive selectivity coefficients (K_{as}) and ion-imprinting factors (IIF) by the following equations.

$$K_{ad} = \frac{Q_e}{C_e} \tag{3}$$

$$K_{as} = \frac{K_{ad-Cu(II)}}{K_{ad(\ competitive\ \ ion\ )}} \tag{4}$$

$$IIF = \frac{K_{as(imprinted)}}{K_{as(non-imprinted)}} \tag{5}$$

Anti-inference stability

The 0.05 g IBCN-Cu adsorbent was immersed into 100 mL 10 mg/L Cu(II) solution containing 100 mg/L interference ions including Na(I), K(I), Ca(II), Mg(II) and Fe(III) at pH = 6.0 with temperature of 298 K by the batch method. The anti-inference stability of the IBCN-Cu was evaluated by comparing the Cu(II) adsorption capacity.

Reusability performance

The reusability of the IBCN-Cu nonwoven adsorbent was characterized by the adsorption/desorption circle under a constant pH of 5.0 and at 298 K. The saturated IBCN-Cu after adsorption was regenerated with 1.0 mol/L HCl solution to extract Cu(II) ions from adsorbent. Then, the IBCN-Cu nonwoven adsorbent was neutralized by water and 0.1 mol/L NaOH solution and dried under vacuum overnight. After that, the regenerated IBCN-Cu nonwoven adsorbent was reused for subsequent re-adsorption process. This adsorption/desorption circle was repeated for ten times to reveal the stability and reusability performance of the as-obtained IBCN-Cu.

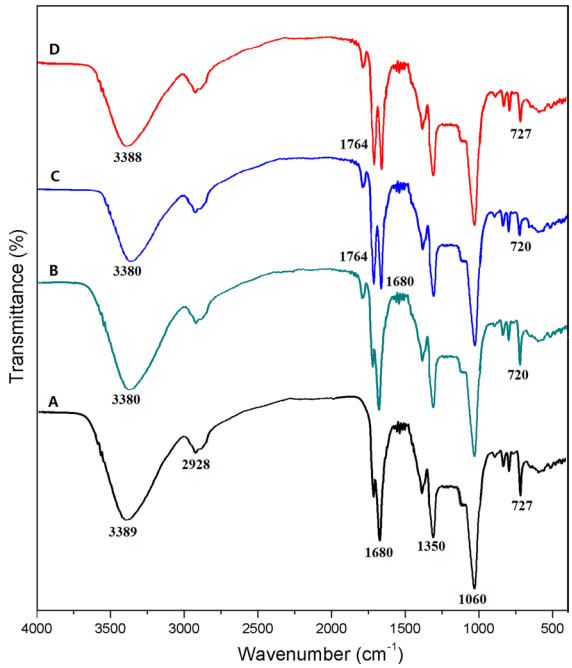

Fig. 1 FTIR spectra of surface imprinted BC nanofiber nonwoven fabric adsorbent at different preparation stages

Result and discussion

FT-IR spectra

Figure 1 shows FT-IR spectra of each stage in the preparation of surface Cu(II) imprinted BC nanofiber nonwoven fabric adsorbent. A is spectrum of BC nanofiber nonwoven fabric (BNNF), B is spectrum of Cu(II) ions mixed with BNNF (BNNF-Cu), C is spectrum of cross-linked BNNF-Cu, and D is spectrum of surface Cu(II) imprinted BC nanofiber nonwoven fabric adsorbent (IBCN-Cu). As seen in spectrum A for BNNF, the broad absorption band at 3389 cm^{-1} is ascribed to the –OH stretching vibrations. Absorption band at 2928 cm^{-1} represents the stretching vibration of aliphatic C–H. Absorption bands at 1680 cm^{-1} and 1352 cm^{-1} are assigned to the hydrogen-bonded carbonyl stretching vibration and CH_2 symmetric bending vibration,

respectively. The absorption band at 1060 cm^{-1} is attributed to the presence of C–O–C stretching vibrations. The absorption band at 727 cm^{-1} is due to –OH out-of-phase bending vibrations. In the spectrum of BNNF-Cu, the –OH stretching vibration band has shifted to 3380 cm^{-1} and –OH bending vibration band moves to 720 cm^{-1}. Generally, the bond force constant of –OH group will increase after bonding with positively charged ions, which may result in longer bond length and lower absorption band wavenumber. This result suggests that the Cu(II) ions were coordinated with the hydroxyl groups to form chelation of Cu(II) ions in the BNNF-Cu. After crosslinking reaction, the –OH stretching vibration band at 3380 cm^{-1} and –OH bending vibration band at 720 cm^{-1} become weaker. A new absorption band detected at 1764 cm^{-1} is attributed to carbonyl group of the acetal, suggesting that –OH groups react with glutaraldehyde to form crosslinked BNNF-Cu. The crosslinking of –OH groups on the surface of BC nanofibers results in the formation of imprinted cavities. In the spectrum D for IBCN-Cu nonwoven fabric adsorbent, the ratio of –OH stretching vibration band and bending vibration band is improved compared with that of in the spectrum C, together with the –OH stretching vibration and bending vibration bands moving to 3388 and 727 cm^{-1}, indicating that Cu(II) ions are removed by HCl elution. Thus, the surface imprinted BC nanofiber nonwoven fabric adsorbent with free imprinted cavities can be formed. The positions of the major characteristic bands have little change, implying that the chemical composition and overall structure are rather stable during ion-imprinting process including adsorption, crosslinking and elution stages. It can be concluded

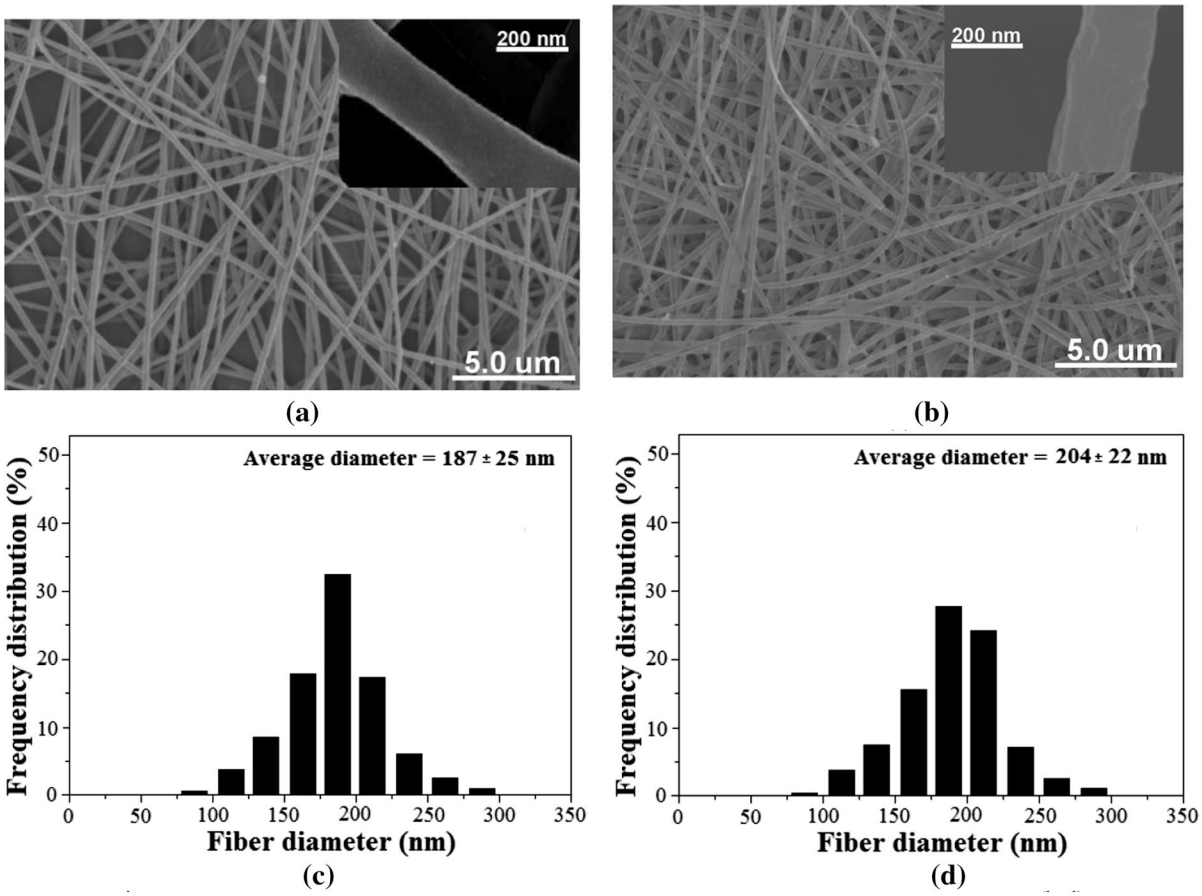

Fig. 2 SEM image and fiber diameter distribution curve for BNNF (**a**, **c**) and IBCN-Cu (**b**, **d**)

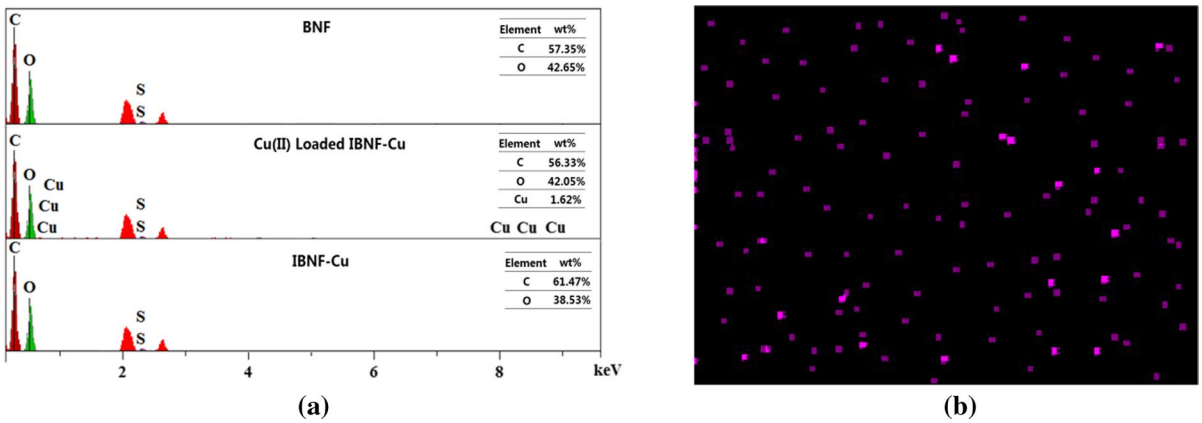

Fig. 3 EDX spectra of BNF, Cu(II) loaded IBCN-Cu and IBCN-Cu adsorbent (**a**); Cu map showing Cu(II) distribution in Cu(II) loaded IBCN-Cu adsorbent (**b**)

that the fabrication process of the surface Cu(II) imprinted BC nanofiber nonwoven fabric adsorbent is feasible by a comprehensive comparison of FT-IR spectrum of each preparation stage.

Surface morphology

Figure 2 displays the morphological analysis of BC nanofiber nonwoven fabric (BNNF) and surface Cu(II) imprinted BC nanofiber nonwoven fabric adsorbent (IBCN-Cu) by scanning electron microscope (SEM), together with the fiber diameter distribution curves calculated by Photoshop software. Evidently, BC nanofiber presents smooth surface with round shape. The arrangement of nanofibers is random to form three-dimensional network structure with interconnected pore structure and high porosity (Fig. 2a). The fiber diameter is rather uniform with the value in the range of 150–250 nm (Fig. 2b). After ion imprinting, IBCN-Cu demonstrates denser with a more rigid structure due to the existence of metal-hydroxyl complex coordination (Fig. 2c). There is few changes in fiber diameter distribution curve (Fig. 2d), while nanofiber surface turns rougher. The rougher surface can provide larger specific surface areas (245.54 m^2/g) than that of BNNF (176.82 m^2/g), meaning higher metal ion adsorption capacity owing to the mass transfer rate of metal ions toward the nanofiber surface.

EDX study

The surface composition and element location of the BNF, Cu(II) loaded IBCN-Cu and IBCN-Cu nonwoven adsorbent was investigated by EDX analysis. As presented in Fig. 3a, only carbon (C) and oxygen (O) element can be detected for BNF owing to its chemical unit structure ($C_6H_{10}O_5$). The presence of Cu(II) in the Cu(II) loaded IBCN-Cu was confirmed by the spectra. Cu map showing the distribution of the Cu element (purple points) on the surface of Cu(II) loaded IBCN-Cu adsorbent after adsorption process was demonstrated in Fig. 3b. For IBCN-Cu nonwoven adsorbent, no Cu element can be detected, which means that Cu(II) ions were removed out completely during acid treatment. Almost the same content of C and N detected in all spectra reveal that the BC remained intact in IBCN-Cu and Cu(II) loaded IBCN-Cu.

Optimization of fabrication process parameters

The IBCN-Cu was prepared using two-step process combined electrospinning technique with SIIM including nanofiber fabrication, ions adsorption, crosslinking and ions elution stages. To optimize the fabrication process, the effect of various preparation parameters on the Cu(II) adsorption were systematically assessed on IBCN-Cu.

In nanofiber fabrication stage, to evaluate the electrospinning technique, different parameters like applied voltage (18, 20, 22 and 25 kV), exclusion

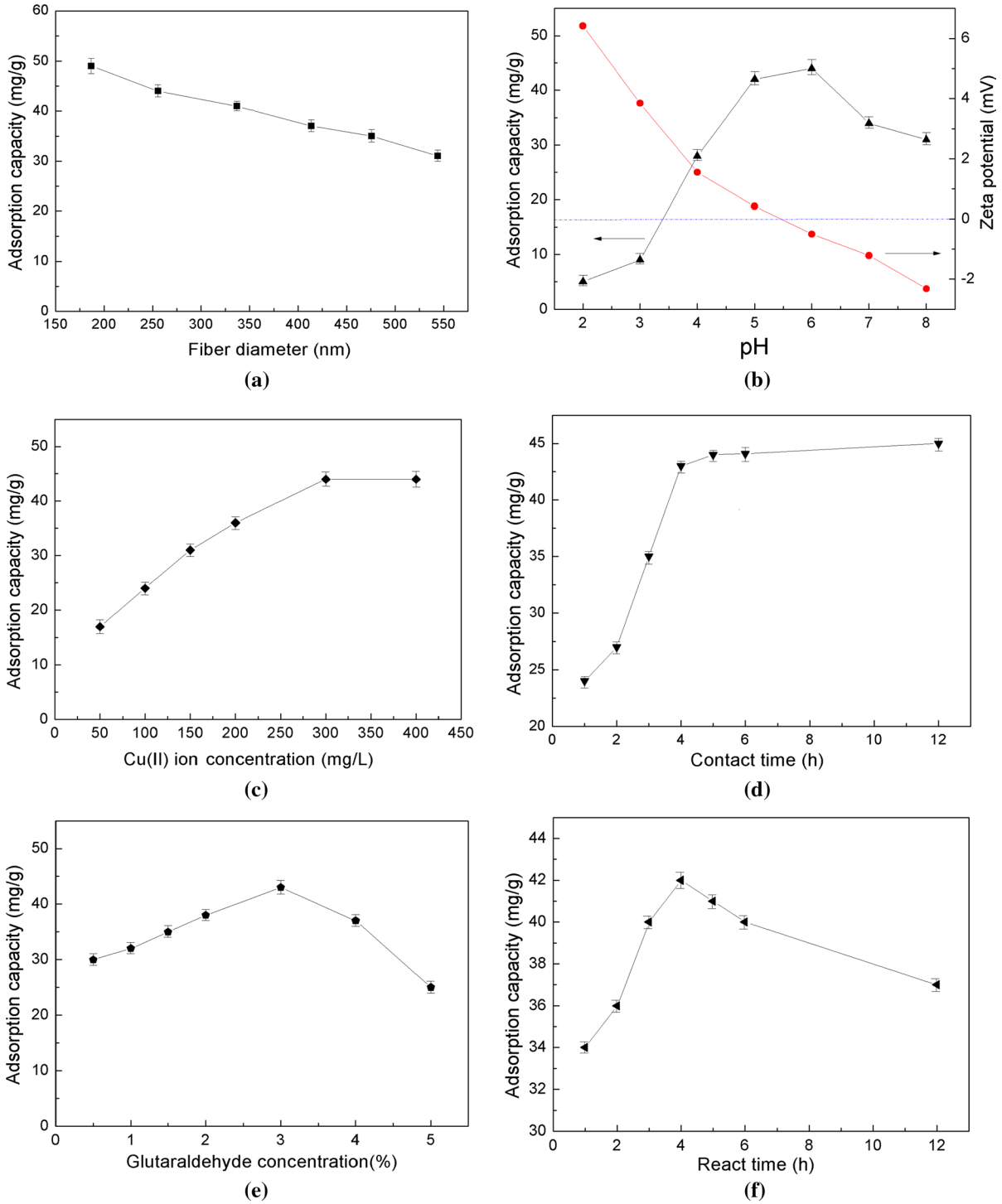

Fig. 4 Effects of **a** fiber diameter, **b** pH value, **c** Cu(II) ion concentration, **d** contact time, **e** glutaraldehyde concentration, **f** react time, **g** HCl concentration and **h** extraction time on the Cu(II) adsorption of IBCN-Cu (Each of the adsorption experiment was repeated for 3 times to reduce errors)

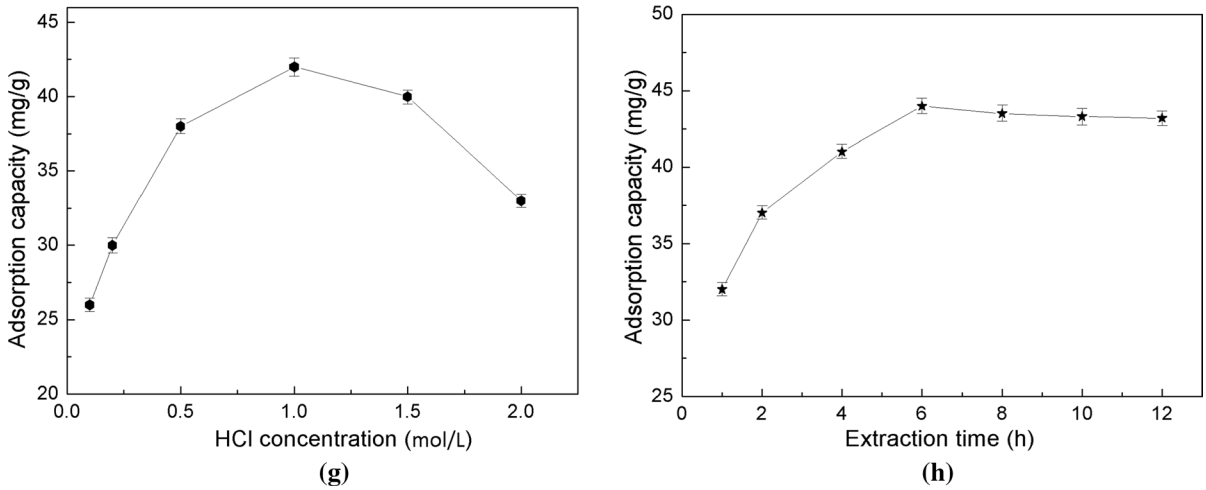

Fig. 4 (continued)

speed (0.5, 1.0, 1.5 and 2.0 mL/h) and collecting distance (18, 20, 22 and 25 cm) were investigated in the preparation of IBCN-Cu. Using orthogonal experiment, fiber average diameter ranged from 187 ± 25 to 544 ± 47 can be fabricated. The Cu(II) adsorption capacity decreases with the increase of fiber diameter as shown in Fig. 4a. This phenomenon should result from the specific surface area of nanofiber adsorbent, which is in favor of the fixation of the ion-imprinted cavities. Higher specific surface area can form more recognition sites for selective adsorption of target ions. Thus, the optimal electrospinning parameters are applied voltage of 25 kV, exclusion speed of 1.0 mL/h and collecting distance of 22 cm, resulting in the finest nanofibers with average diameter of 187 ± 25 nm.

In ion adsorption stage, the concentration of Cu(II) aqueous solution, pH value and contact time were explored to verify the effects on the Cu(II) adsorption of IBCN-Cu by single variable control method. Figure 4b presents the Cu(II) adsorption capacity and zeta potential of IBCN-Cu in the pH value ranged from 2 to 8 adjusted using 0.1 mol/L HCl and 0.1 mol/L NaOH aqueous solutions. The Cu(II) adsorption capacity rises up to the maximum at 6.0 with pH value increased, and then it declines gradually. It obviously shows a pH-dependent adsorption behavior due to chelation reactions which are also pH sensitive. The reason might be attributed to the zeta potential of IBCN-Cu as presented in Fig. 4b. At the pH value lower than 5.5, the positive net charge of IBCN-Cu may cause electrostatic repulsion to Cu(II) ions, leading to the decrease of Cu(II) ion adsorption. When the pH value is lower than 2.0, the strong electrostatic repulsion between protonated hydroxyl groups of IBCN-Cu and the positively charged Cu(II) ions greatly reduce the chelating ability of hydroxyl groups towards Cu(II) ions. At the pH value higher than 5.5, the negative net charge of IBCN-Cu may cause electrostatic attraction to Cu(II) ions, leading to the increase of Cu(II) ion adsorption. However, the transformation from Cu(II) ions to $Cu(OH)_2$ and precipitates would happen, which resulting in the decrease of Cu(II) ion adsorption. Consequently, the suitable pH region for IBCN-Cu to adsorb Cu(II) ions is 5.5–6.5 and 6.0 is set to the optimal pH value for all the adsorption experiments.

Figure 4c, d demonstrate the effect of the concentration of Cu(II) aqueous solution and contact time on Cu(II) adsorption of IBCN-Cu. The equilibrium adsorption is achieved with the concentration of Cu(II) aqueous solution ranged from 50 to 400 mg/L. The Cu(II) adsorption capacity enhances firstly with the increasing of the concentration of Cu(II) aqueous solution as well as contact time and then levels off. This result comes from the competition between free Cu(II) ions and recognition sites. Normally, Cu(II) ion adsorption involves two stages. In the first stage, a large amount of free recognition sites available for Cu(II) ion adsorption and adsorption rate is swift. In the second stage, Cu(II) ion adsorption rate reduces gradually and achieve to equilibrium in the end

because of depletion of recognition sites or Cu(II) ions in aqueous solution. Thus, the optimal Cu(II) ion concentration and contact time in ion adsorption stage are 300 mg/L and 5 h, respectively.

In the crosslinking stage, the concentration of glutaraldehyde aqueous solution and react time were investigated to testify the influences on the Cu(II) adsorption of IBCN-Cu as presented in Fig. 4e, f. The Cu(II) adsorption capacity increases when the glutaraldehyde concentration is less than 3%. Then an obvious decrease was presented when the glutaraldehyde concentration is over 3%. As for react time under 3% glutaraldehyde concentration, the maximum adsorption capacity appears at about 4 h. During the crosslinking stage, the hydroxyl functional groups can react with glutaraldehyde to form crosslinking structure by acetal. The higher crosslinking structure may limit the formation of effective recognition sites, which result in the attenuation of Cu(II) ion adsorption capacity.

In ion elution stages, extraction process is the critical step for IBCN-Cu preparation, which directly affect the adsorption capacity and selectivity. To optimize the eluent concentration, the Cu(II) ions was extracted by HCl aqueous solutions with the concentration ranged from 0.1 to 2.0 mol/L. The adsorption capacity increases with the eluent concentration increasing from 0.1 to 1.0 mol/L and slightly decreases after 1.0 mol/L, as presented in Fig. 4g. The decline in adsorption capacity might be ascribed to the excessive concentration of HCl, which can destroy the recognition sites of IBCN-Cu. Choosing 1.0 mol/L HCl as the eluent, the effect of extraction time on adsorption capacity was investigated and the result is shown in Fig. 4h. When the extracting time is less than 6 h, the adsorption capacity present an increasing tendency with extraction time increasing. The increasing extraction time is in favor of Cu(II) ion extraction, which results in an increasing of recognition sites until saturation before 6 h. Then, the adsorption capacity shows a plateau with slight decline after 6 h, resulting from the recognition sites damaged during the excessive extraction.

Adsorption isotherms of IBCN-Cu

The ion-imprinting effect on selective adsorption of IBCN-Cu was explored by adsorption isotherm. The isothermal adsorption experiments were performed using different metal ions (Cu(II), Zn(II), Ni(II), Pb(II), Cd(II)) under concentrations ranged from 10 to 500 mg/L at pH = 6.0 with temperature of 298 K. As demonstrate in Fig. 5a, the adsorption capacity of IBCN-Cu toward all metal ions presents an incremental tendency with the concentration increased, and then tends to be saturated.

To investigate the adsorption mechanism of IBCN-Cu, the experimental data are then fitted with Langmuir and Scatchard isotherm model, respectively. The Langmuir and Scatchard isotherm model can be mathematically expressed using Eqs. (6) and (7).

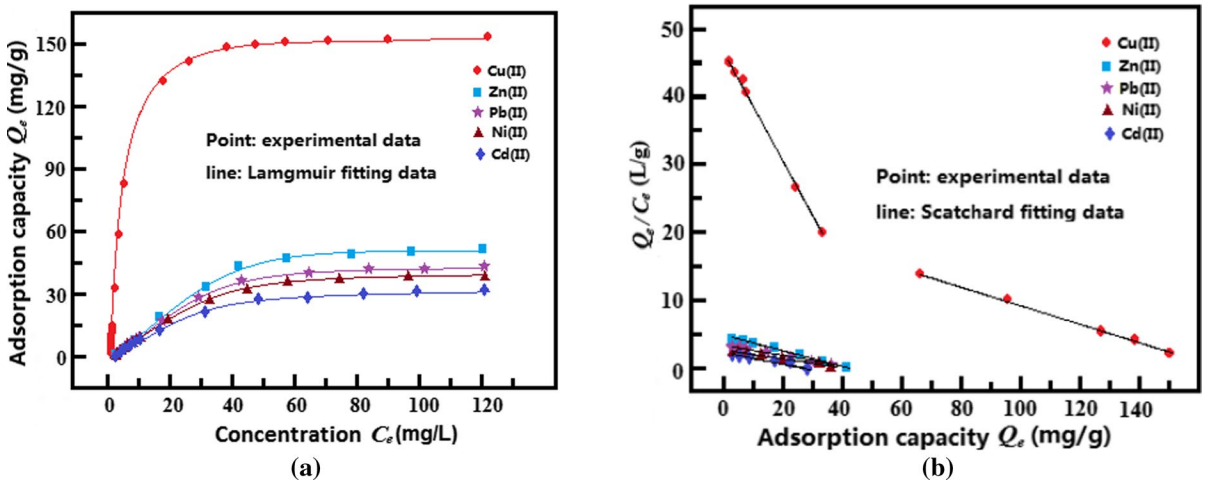

Fig. 5 Langmuir isotherm model, **a** and Scatchard isotherm model, **b** for Cu(II), Zn(II), Pb(II) and Cd(II) adsorption onto IBCN-Cu

$$\frac{Q_e}{C_e} = \frac{C_e}{Q_m} + \frac{1}{K_L \times Q_m} \tag{6}$$

$$\frac{Q_e}{C_e} = \frac{(Q_m - Q_e)}{K_S} \tag{7}$$

where Q_m (mg/g) represents the maximum adsorption capacity, K_L (L/mg) and K_s (mg/L) are the Langmuir adsorption coefficient and the equilibrium dissociation constant at recognition sites. Q_e and C_e are same to previous equations.

Obviously. the IBCN-Cu displays a perfect advantage for Cu(II) recognition with the maximum adsorption capacity of 152.2 mg/g, which are about 3–5 times than other metal ions onto IBCN-Cu. The reason may be attributed to the formation of plentiful high-affinity Cu(II)-imprinted sites on the surface of electrospun BC nanofiber based nonwoven fabric.

The fitting curves of Langmuir model for Cu(II), Zn(II), Ni(II), Pb(II) and Cd(II) adsorption by IBCN-Cu are all matched with the experimental data in their own systems, suggesting that the monolayer and symmetrical recognition sites are distributed on the surface of INBF-Cu. The adsorption properties of Zn(II), Ni(II), Pb(II) and Cd(II) by IBCN-Cu are almost same.

In Scatchard model, the fitting curves of Cu(II), Zn(II), Ni(II), Pb(II) and Cd(II) show significant difference. For Cu(II) adsorption, it can be divided into two distinct linear sections with two K_s values, indicating two adsorption stages may happen during the Cu(II) ion recognition by IBCN-Cu. The steep linear section represents specific recognition stage with K_s value of 1.18 mg/L showing higher adsorption affinity, and the flat linear section represents non-specific recognition stage with K_s value of 6.49 mg/L showing lower adsorption affinity. For Zn(II), Ni(II), Pb(II) and Cd(II) adsorption, only one flat linear section with K_s value of 7.33 mg/L, 8.25 mg/L, and 8.77 mg/L and 7.57 mg/L can be fitted. Clearly, non-specific recognition happens for these non-imprinted metal ions due to low adsorption affinity to the recognition sites of IBCN-Cu.

During the surface ion-imprinting process of IBCN-Cu, the Cu(II) ions are firstly bonded with hydroxyl functional groups of BC by chelation reactions, and then form the specific adsorption sites after crosslinking and extraction. Meanwhile, a few number of hydroxyl functional groups are remained to form the non-specific adsorption sites. For Cu(II), both specific adsorption sites and non-specific adsorption sites can adsorbed by IBCN-Cu, which result in two adsorption region in fitting curve of Scatchard model. For non-imprinted metal ions like Zn(II), Ni(II), Pb(II) and Cd(II), specific adsorption adsorption sites can hardly work and only non-specific adsorption sites can adsorb metal ions, forming flat fitting curves with low adsorption capacity. Thus, the specific recognition site should be a key factor for selective adsorption.

Adsorption kinetics of IBCN-Cu

The effect of contact time on the Cu(II) adsorption of IBCN-Cu was further investigated using kinetic models to analyze the mechanism of adsorption process. The dynamic adsorption experiments were carried out with intervals from 10 to 500 min under different initial Cu(II) ion concentration (30, 50 and 100 mg/L) at pH = 6.0 with temperature of 298 K. As presented in Fig. 6a, the variation tendency of adsorption capacity with contact time at different initial concentrations are similar. In the first 60 min, the Cu(II) adsorption capacity increased almost linearly with contact time increasing, and then the increment rate gradually declines. The rapid adsorption at initial time might be attributed to the large number of recognition sites on the surface of IBCN-Cu, which are the specific adsorption sites for Cu(II) with higher affinity. After about 150 min, the Cu(II) adsorption capacity reaches equilibrium. With the initial concentration increasing from 30 to 100 mg/L, the adsorption capacities increases about 225% owing to more Cu(II) available for adsorption by IBCN-Cu. Besides, higher Cu(II) ion concentration can cause more collisions and provide bigger driving force for Cu(II) ions to overcome resistance during the ionic transfer from the aqueous solution to the adsorption sites on the surface of IBCN-Cu.

To study the rate-controlling of Cu(II) adsorption on IBCN-Cu, the obtained dynamic adsorption data are simulated using pseudo-first-order, pseudo-second-order and intra-particle diffusion models, which can be linearly written using Eqs. (8), (9) and (10), respectively.

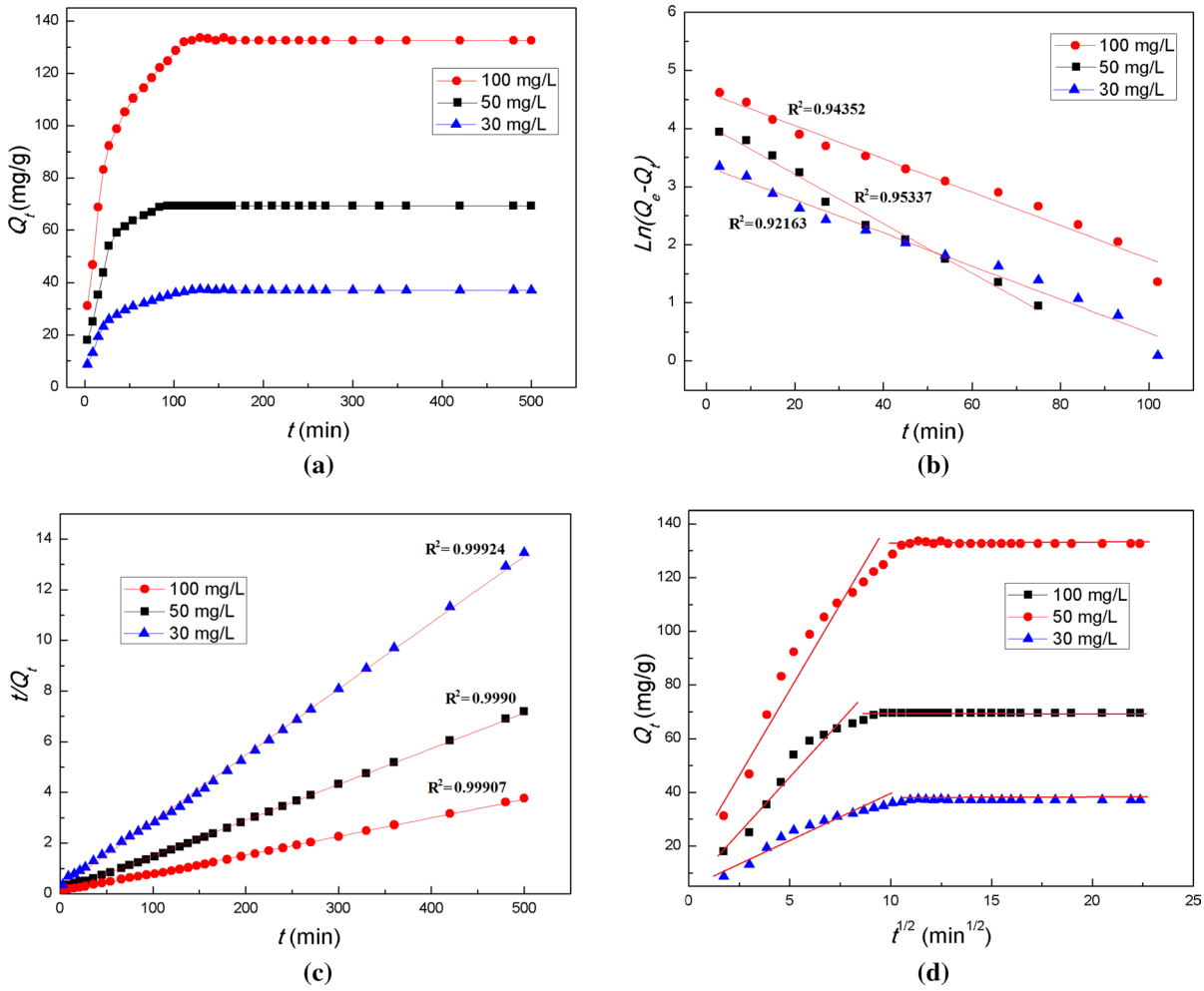

Fig. 6 The effect of contact time on the Cu(II) adsorption of INBF-Cu with the initial Cu(II) concentration of 30, 50 and 100 mg/L (**a**), fitting curves of the pseudo-first order kinetics model (**b**), the pseudo-second order kinetics model (**c**) and the intra-particle diffusion model (**d**)

$$\ln(Q_e - Q_t) = \ln Q_e - \frac{K_1 \times t}{2.303} \tag{8}$$

$$\frac{t}{Q_t} = \frac{1}{K_2 \times Q_e^2} + \frac{t}{Q_e} \tag{9}$$

$$Q_t = K_i t^{0.5} + C \tag{10}$$

where K_1 (L/mg) and K_2 (mg/L) represent rate constants of pseudo-first-order and pseudo-second-order model. K_t (mg/g/min$^{1/2}$) and C denote the intra-particle diffusion rate constant and constant reflecting the boundary layer effect, respectively. Q_e and Q_t are same to previous equations.

As demonstrated in Fig. 6b, c, the linear regression (R^2) of pseudo-second-order is much higher than that of pseudo-first-order, suggesting that the pseudo-second-order kinetic model is more suitable to describe the adsorption process of IBCN-Cu towards Cu(II) ions. Therefore, chemisorption should have an important effect on Cu(II) adsorption on IBCN-Cu, which may be the rate controlling step involving chelation reaction between Cu(II) and IBCN-Cu by electrons sharing. Figure 6d shows the fitting curves of intra-particle diffusion model to verify the steps involved Cu(II) adsorption on

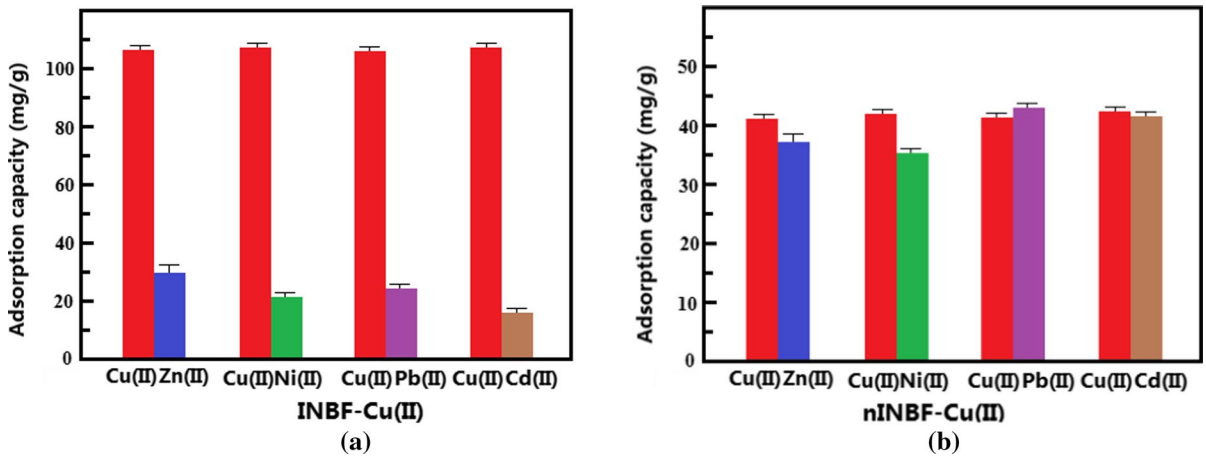

Fig. 7 Competitive adsorption of Cu(II)/Zn(II), Cu(II)/Ni(II), Cu(II)/Pb(II) and Cu(II)/Cd(II) onto IBCN-Cu (**a**) and nIBCN-Cu (**b**)

Table 1 The distribution coefficients (K_{ad}), adsorptive selectivity coefficients (K_{as}) and ion-imprinting factors (*IIF*) for IBCN-Cu and nIBCN-Cu

Ion	$K_{ad\text{-}IBCN\text{-}Cu}$	$K_{ad\text{-}nIBCN\text{-}Cu}$	$K_{as\text{–}IBCN\text{-}Cu}$	$K_{as\text{-}nIBCN\text{-}Cu}$	*IIF*
Cu(II)	19.1	1.09	46.6	1.18	39.5
Zn(II)	0.41	0.92			
Cu(II)	13.9	1.28	37.6	1.32	28.5
Ni(II)	0.37	0.97			
Cu(II)	24.9	0.95	56.6	0.95	59.6
Pb(II)	0.44	1.01			
Cu(II)	19.0	1.11	61.3	1.07	57.3
Cd(II)	0.31	1.04			

IBCN-Cu. The plots can be divided into two linear regions, which indicate two steps may be involved during the whole adsorption process. For the first step, Cu(II) ions show fast transport from bulk solution to surface of IBCN-Cu. For the next step, Cu(II) ions gradually diffuse into the recognition cavities of IBCN-Cu, The linear portions of the lines do not cross the origin with low intra-particle diffusion rate constant (K_t) suggests that intra-particle diffusion is one of the rate limiting step during the Cu(II) adsorption on IBCN-Cu.

Adsorption selectivity of IBCN-Cu

Selective adsorption of the IBCN-Cu was investigated using binary solutions such as Cu(II)/Zn(II), Cu(II)/Ni(II), Cu(II)/Pb(II) and Cu(II)/Cd(II) containing same ion concentration of 50 mg/L at pH = 6.0 with temperature of 298 K by the batch method to investigate recognition ability. Figure 7 depicts the adsorption selectivity performance of IBCN-Cu compared with non ion-imprinted BC nanofiber membrane. For IBCN-Cu, the Cu(II) adsorption capacity is much higher than that of non-imprinted ions, showing a recognition ability in all binary solution system. In case of non ion imprinted BC nanofiber membrane, there is only small difference in adsorption capacity between Cu(II) and other competitive ions in the same binary system. The distribution coefficients (K_{ad}), adsorptive selectivity coefficients (K_{as}) and ion-imprinting factors (*IIF*) are calculated to estimate the adsorption selectivity of IBCN-Cu and the results are listed in Table 1.

Apparently, the $K_{ad\text{-}IBCN\text{-}Cu}$ is much higher than $K_{ad\text{-}nIBCN\text{-}Cu}$, and the $K_{ad\text{-}Cu(II)}$ values of IBCN-Cu is rather higher than $K_{ad\text{-}Zn(II)}$, $K_{ad\text{-}Ni(II)}$, $K_{ad\text{-}Pb(II)}$ and $K_{ad\text{-}Cu(II)}$ of IBCN-Cu. Thus, high adsorptive selectivity coefficients (K_{as}) are determined for the IBCN-Cu: 46.6, 37.6, 56.6 and 61.3 for Cu(II)/Zn(II), Cu(II)/Ni(II), Cu(II)/Pb(II) and Cu(II)/Cd(II), reflecting

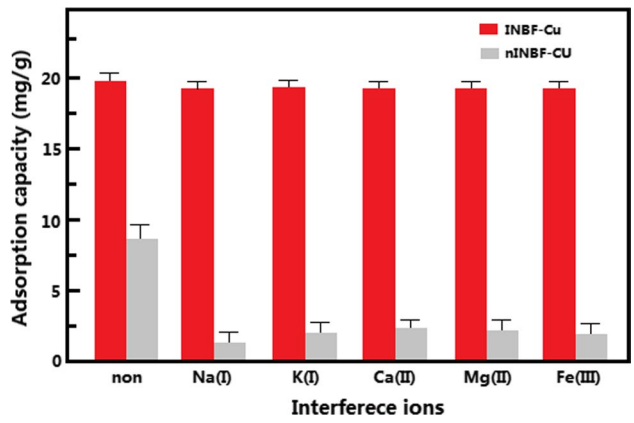

Fig. 8 Anti-interference ability of IBCN-Cu

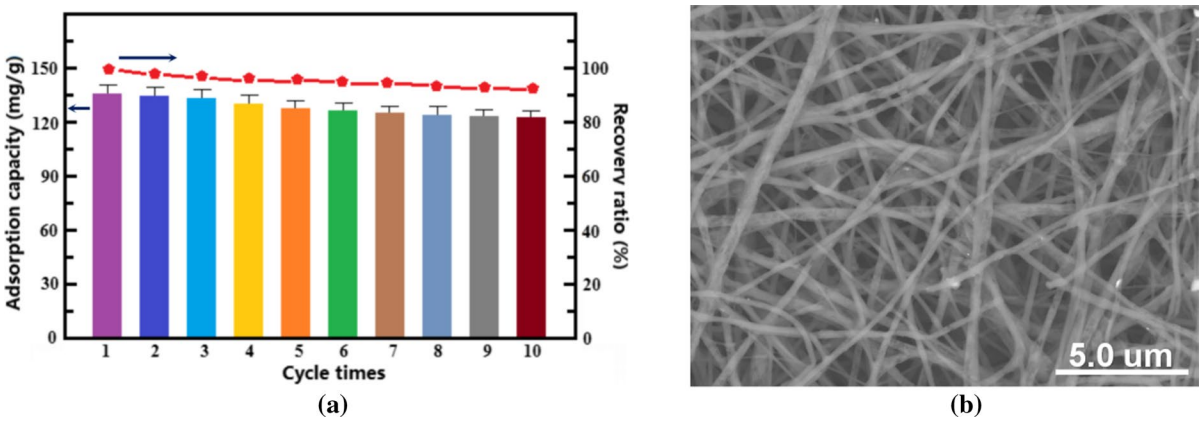

Fig. 9 Reusability performance of the IBCN-Cu (**a**) and SEM image after 10 regeneration cycles (**b**)

great adsorption selectivity of IBCN-Cu for Cu(II) ions. Moreover, *IIF* values of Cu(II)/Zn(II), Cu(II)/Ni(II), Cu(II)/Pb(II) and Cu(II)/Cd(II) binary system are 39.5, 28.5, 59.6 and 57.3, indicating that ion-imprinting process can remarkably improve recognition selectivity of adsorbents. These results might be due to the well-designed ion-imprinted recognition sites with coordination geometry matching with Cu(II) ions in charge, size, shape, coordination number and spatial arrangement of hydroxyl groups. The IBCN-Cu possesses a great selectivity and recognition for Cu(II) in various competitive ion systems by means of the imprinted adsorption sites with specific recognition selectivity towards Cu(II) ions.

Anti-interference ability of IBCN-Cu

Generally, the commonly present metal cation ions in natural water like Na(I), K(I), Ca(II), Mg(II) and Fe(III) may play a negative interference effect on Cu(II) adsorption by IBCN-Cu. To investigate the anti-interference ability of IBCN-Cu, the Cu(II) removal efficiency was explored in the mixture solution with the concentration of interference ion 10 times higher than that of Cu(II) ion. As given in Fig. 8, there is a slight reduction (<5%) in Cu(II) removal efficiency in the presence of Na(I), K(I), Ca(II), Mg(II) and Fe(III) with high concentration, indicating that these interference ions hardly affect Cu(II) adsorption on IBCN-Cu by competing adsorption sites with Cu(II) ions. As a result, IBCN-Cu shows high selective Cu(II) removal efficiency with excellent anti-interference ability.

Stability and reusability of IBCN-Cu

For nanofiber nonwoven adsorbents, stability and reusability performance are the key factors

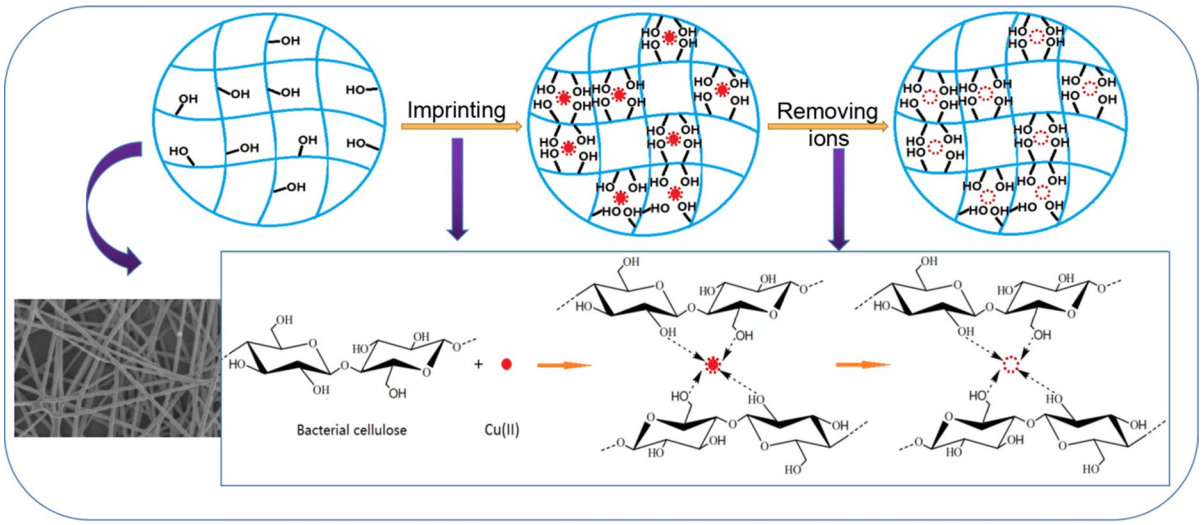

Fig. 10 Adsorption mechanism of IBCN-Cu for Cu(II)

determining their economic value for potentially practical applications. Therefore, the IBCN-Cu was subjected to regeneration cycles (adsorption/desorption) for 10 times with time interval of 12 h. Figure 9a illustrates the variation of adsorption capacity and recovery ratio with regeneration cycles for Cu(II) adsorption on IBCN-Cu. The adsorption capacity of IBCN-Cu presents no obvious decrease with cycling, and the recovery ratio of IBCN-Cu reaches up to 92.1% of the initial adsorption after 10 cycles of reuse. Observed by SEM image (Fig. 9b), the surface morphology of IBCN-Cu does not show remarkable difference only with slight nanofiber damage after ten cycles of adsorption/desorption. The results confirm that the as-obtained IBCN-Cu possesses physical/chemical stability and excellent regeneration performance, which could be a promising potential as Cu(II) adsorbent for practical applications.

Adsorption mechanism of IBCN-Cu absorbent

Based on the adsorption isotherm and kinetic results, it can be concluded that the adsorption of Cu(II) by IBCN-Cu absorbent is chemisorption in nature, which might involve formation of valence forces by chelation through coordination between the Cu(II) (electron-accepting nature) and hydroxyl functional groups of BC (O-containing groups on the surface, electron donating nature), as illustrated in Fig. 10. After removing Cu(II), specific adsorption sites can be formed in IBCN-Cu absorbent, which match with Cu(II) ions in charge, size, shape, coordination number and spatial arrangement of hydroxyl groups. These specific adsorption sites result in high recognition selectivity and anti-interference ability for Cu(II).

Comparison of IBCN-Cu absorbent

The comparison of as-prepared IBCN-Cu adsorbent with other previously reported Cu(II) imprinted adsorbents including preparation method, adsorbent type, adsorption capacity and recognition selectivity is summarized in Table 2. Clearly, the IBCN-Cu presents higher performance in adsorption capacity, recognition selectivity and anti-interference ability for Cu(II) ion than most of other adsorbents, which reflects the advantages of the prepared material as an adsorbent. However, the complex two-step preparation process including electrospinning and surface ion-imprinted technology would cause the instability of the materials, which might be the disadvantages of the IBCN-Cu as an adsorbent. Thus, one-step method to prepare IBCN-Cu absorbent is ongoing in our lab and will be reported later.

Table 2 Comparison of Cu(II) ion-imprinted adsorbents in the reported literature

Adsorbent	Preparation method	Type	Adsorption capacity	Selectivity performance (selectivity coefficients)				References
				Cu(II)/Zn(II)	Cu(II)/Ni(II)	Cu(II)/Pb(II)	Cu(II)/Cd(II)	
Cu(II) imprinted gelatin/8-hydroxyquinoline/chitosan copolymer	Bulk polymerization	Film	111.81 mg/g	> 18.71	> 18.71	> 18.71	> 18.71	Wang et al. (2019a, b)
Cu(II) imprinted porous polymethacrylate	Suspension polymerization	Micro-particles	235 μmol/g	42.38	43.38	–	–	Hoai et al. (2010)
Cu(II) imprinted methacrylic acid based copolymer	Precipitation polymerization	Nanobeads	38.8 mg/g	16.8	14.1	32.4	–	Roushani et al. (2015)
Cu(II) ion-imprinted polymer using ethylene glycol dimethacrylateas functional monomer	Precipitation method	Particles	14.8 mg/g	6.57	126	–	–	Pang et al. (2011)
Cu(II) ion-imprinted polymer using *N*-[3-(2-aminoethylamino) propyl] trimethoxysilane as functional monomer	Sol–gel process	–	39.82 mg/g	–	–	2.65	55.64	Ren et al. (2018)
Cu(II) ion-imprinted chitosan/attapulgite polymer	Sol–gel process	Packed fibers	35.2 mg/g	–	–	78.45	82.44	Cai et al. (2014)
Cu(II) ion-imprinted Fe_3O_4@SiO_2 adsorbent	Sol–gel process	Micro-particles	24.2 mg/g	91.84	133.92	–	–	Zhu, et al. (2011)
Cu(II) imprinted Chitosan biosorbent	Microfluidic technology	Micro-particle	81.97 mg/g	1.78	–	6.35	–	Zhu et al. (2017)

Table 2 (continued)

Adsorbent	Preparation method	Type	Adsorption capacity	Selectivity performance (selectivity coefficients)				References
				Cu(II)/Zn(II)	Cu(II)/Ni(II)	Cu(II)/Pb(II)	Cu(II)/Cd(II)	
Cu(II) imprinted tetraethylene pentamine modified active carbon	Grafting	Sphere	33.33 mg/g	36.07	38.64	–	31.82	Peng et al. (2015)
Cu(II) imprinted chitosan / Fe_3O_4 nanoparticles composite adsorbent	Metal imprinting	Micro-particle	71.36 mg/g	2.8	5.73	–	–	Janmohammadi et al. (2018)
Cu(II) imprinted silica gel sorbent	Surface imprinting	Mesoporous gel	84.5 μmol/g	12.3	–	–	-	Wu et al. (2010)
Cu(II) ion-imprinted chitosan/epichlorohydrin adsorbent	Ion-imprinting method	Micro-particles	21.12 mg/g	1.91	0.97	–	–	Chen et al. (2011)
Cu(II) ion-imprinted Polyethyleneimine based polymer	Ion-imprinted technology	Porous particles	83.3 mg/g	0.96	22.38	15.16	–	Duan et al. (2017)
Cu(II) ion-imprinted BC nanofiber nonwoven	Surface ion-imprinting	Nanofiber nonwoven	152.2 mg/g	46.6	37.6	56.6	61.3	This work

Conclusion

In summary, a novel surface Cu(II) ion-imprinted bacterial cellulose nanofiber nonwoven adsorbent (IBCN-Cu) was successfully prepared by surface ion-imprinting technique combined with electrospinning technology. The obtained IBCN-Cu presents excellent adsorption ability with the maximum adsorption capacity of 152.2 mg/g at 298 K. The Cu(II) adsorption process can be well described by Langmuir model and pseudo-second order kinetic model. The selectivity coefficients for Cu(II) adsorption on IBCN-Cu in binary metal solution of Cu(II)/Zn(II), Cu(II)/Ni(II), Cu(II)/Pb(II) and Cu(II)/Cd(II) reach up to 47, 101, and 162, respectively. The ion-imprinting factor (IIF) values of Cu(II)/Zn(II), Cu(II)/Ni(II), Cu(II)/Pb(II) and Cu(II)/Cd(II) binary system are 39.5, 28.5, 59.6 and 57.3, indicating that ion-imprinting process can remarkably improve recognition selectivity of adsorbents. As illustrated by Scatchard model, the specific recognition site with high Cu(II) affinity should be a key factor affecting selective adsorption. In addition, the IBCN-Cu exhibits good

anti-interference ability and reusability. The IBCN-Cu can be reused at least ten cycles with only 7.9% reduction in adsorption capacity. As a conclusion, the Cu(II)-imprinted nanofiber nonwoven prepared in this work can be considered to be an effective and reliable adsorbent for the separation and enrichment of Cu(II) ions in environmental water samples.

Funding This work was supported by Tianjin Science Technology Research Funds of China (19JCZDJC37500). We would like to thank the Analytical & Testing Center of Tiangong University for structured illumination microscopy work.

Declarations

Conflict of interest The authors declare that they have no conflict of interest.

References

Abdi J, Vossoughi M, Mahmoodi NM, Alemzadeh I (2017) Synthesis of amine-modified zeolitic imidazolate framework-8, ultrasound-assisted dye removal and modeling. Ultrason Sonnchem 39:550–564

Bakhshpour M, Tamahkar E, Anda M, Denizli A (2017) Surface imprinted bacterial cellulose nanofibers for hemoglobin purification. Coll Surf B 158:453–459

Bashir A, Malik LA, Ahad S, Manzoor T, Bhat MA, Dar GN (2019) Removal of heavy metal ions from aqueous system by ion-exchange and biosorption methods. Environ Chem Lett 17:729–754

Bhagat SK, Tung TM, Yaseen ZM (2020) Development of artificial intelligence for modeling wastewater heavy metal removal: state of the art, application assessment and possible future research. J Clean Prod 250:119473

Cai XQ, Li JH, Zhang Z, Yang FF, Dong RC, Chen LX (2014) Novel Pb^{2+} ion imprinted polymers based on ionic interaction via synergy of dual functional monomers for selective solid-phase extraction of Pb^{2+} in water samples. Appl Mater Interfaces 6:305–313

Chen CY, Yang CY, Chen AH (2011) Biosorption of Cu(II), Zn(II), Ni(II) and Pb(II) ions by crosslinked metal-imprinted chitosans with epichlorohydrin. J Environ Manag 92:796–802

Chen Q, Yao Y, Li X, Lu J, Zhou J, Huang Z (2018) Comparison of heavy metal removals from aqueous solutions by chemical precipitation and characteristics of precipitates. J Water Process Eng 26:289–300

Chen X, Cui J, Xu X, Sun B, Sun D (2019) Bacterial cellulose/attapulgite magnetic composites as an efficient adsorbent for heavy metal ions and dye treatment. Carbohydr Polym 229:115512

Davarpanah S, Mahmoodi NM, Arami M, Bahrami H, Mazaheri F (2009) Environmentally friendly surface modification of silk fiber: chitosan grafting and dyeing. Appl Surf Sci 255:4171–4176

Duan JX, Li X, Zhang CC (2017) The synthesis and adsorption performance of polyamine Cu^{2+} imprinted polymer for selective removal of Cu^{2+}. Polym Bull 74:3487–3504

Emel T, Monireh B, Adil D (2019) Molecularly imprinted composite bacterial cellulose nanofibers for antibiotic release. J Biomat Sci Polym E 30(6):450–461

Erol K, Uzun L (2017) Two-step polymerization approach for synthesis of macroporous surface ion-imprinted cryogels. J Macromol Sci A 54(11):867–875

Fang Q, Zhou X, Deng W, Zheng Z, Liu Z (2016) Freestanding bacterial cellulose-graphene oxide composite membranes with high mechanical strength for selective ion permeation. Sci Rep 6(1):33185

He HX, Gan Q, Feng CG (2018) An ion-imprinted silica gel polymer prepared by surface imprinting technique combined with aqueous solution polymerization for selective adsorption of Ni(II) from aqueous solution. Chin J Polym Sci 36:51–60

Hoai NT, Yoo D, Kim D (2010) Batch and column separation characteristics of copper-imprinted porous polymer micro-beads synthesized by a direct imprinting method. J Hazard Mater 173:462–467

Hong HJ, Lim JS, Hwang JY, Kim M, Jeong HS, Park MS (2018) Carboxymethlyated cellulose nanofibrils(CMCNFS) embedded in polyurethane foam as a modular adsorbent of heavy metal ions. Carbohydr Polym 195:136–142

Hou Y, Wang X, Yang J, Zhu R, Li Y (2018) Development and biocompatibility evaluation of biodegradable bacterial cellulose as a novel peripheral nerve scaffold. J Biomed Mater Res A 106:1288–1298

Janmohammadi M, Nourbakhsh MS (2018) Electrospun polycaprolactone scaffolds for tissue engineering: a review. Int J Polym Mater Po 68:1–13

Jiajia W, Zhanwen D, Ping X, Zhijiang C (2020) Fabrication of flexible polyindole/carbon nanotube/bacterial cellulose nanofiber nonwoven electrode doped by D-tartaric acid with high electrochemical performance. Cellulose 27:6353–6366

Kashefi S, Borghei SM, Mahmoodi NM (2019) Covalently immobilized laccase onto graphene oxide nanosheets: preparation, characterization, and biodegradation of azo dyes in colored wastewater. J Mol Liq 276:153–162

Kim T, Kim TK, Zoh KD (2020) Removal mechanism of heavy metal (Cu, Ni, Zn, and Cr) in the presence of cyanide during electrocoagulation using Fe and Al electrodes. J Water Process Eng. 33:101109

Li Z, Tian H, Yuan Y, Yin X, Wei X, Tang L et al (2019) Metal-ion-imprinted thermo-responsive materials obtained from bacterial cellulose: synthesis, characterization, and adsorption evaluation. J Mater Chem A 7:11742–11755

Mahmoodi NM (2014) Binary catalyst system dye degradation using photocatalysis. Fiber Polym 15(2):273–280

Mahmoodi NM, Arami M, Limaee NY, Gharanjig K, Nourmohammadian F (2007) Nanophotocatalysis using immobilized titanium dioxide nanoparticle: degradation and mineralization of water containing organic pollutant—case study of Butachlor. Mater Res Bull 42:797–806

Miao YE, Zhu GN, Hou H, Xia YY, Liu T (2013) Electrospun polyimide nanofiber-based nonwoven separators for lithium-ion batteries. J Power Sources 226:82–86

Mishra S, Verma N (2017) Surface ion imprinting-mediated carbon nanofiber-grafted highly porous polymeric beads: synthesis and application towards selective removal of aqueous Pb(II). Chem Eng J 313:1142–1151

Monier M, Abdel-Latif DA (2013) Synthesis and characterization of ion-imprinted resin based on carboxymethyl cellulose for selective removal of Uo_2^{2+}. Carbohydr Polym 97:743–752

Mousavi S, Deuber F, Petrozzi S, Federer L, Aliabadi M, Shahraki F, Adlhart C (2018) Efficient dye adsorption by highly porous nanofiber aerogels. Colloid Surf A 547:117–125

Nasrollahi N, Aber S, Vatanpour V, Mahmoodi NM (2019) Development of hydrophilic microporous PES ultrafiltration membrane containing CuO nanoparticles with improved antifouling and separation performance. Mater Chem Phys 222:338–350

Ngah WSW, Teong LC, Hanafiah MAKM (2011) Adsorption of dyes and heavy metal ions by chitosan composites: a review. Carbohydr Polym 83:1446–1456

Pang Y, Zeng GM, Tang L, Zhang Y, Liu YY, Lei XX, Li Z, Zhang JC, Xie GX (2011) PEI-grafted magnetic porous powder for highly effective adsorption of heavy metal ions. Desalination 281:278–284

Peng W, Xie ZZ, Cheng G, Shi L, Zhang YB (2015) Amino-functionalized adsorbent prepared by means of Cu(II) imprinted method and its selective removal of copper from aqueous solutions. J Hazard Mater 294:9–16

Quan F, Dingsheng W, Yong Z, Anfang W, Qufu W, Hao F (2018) Electrospun AOPAN/RC blend nanofiber membrane for efficient removal of heavy metal ions from water. J Hazard Mater 344:819–828

Ren ZQ, Zhu XY, Du J, Kong DL, Wang N, Wang Z, Wang Q, Liu W, Li QS, Zhou ZY (2018) Facile and green preparation of novel adsorption materials by combining sol-gel with ion imprinting technology for selective removal of Cu(II) ions from aqueous solution. Appl Surf Sci 435:574–584

Roushani M, Abbasi S, Khani H (2015) Synthesis and application of ion-imprinted polymer nanoparticles for the extraction and preconcentration of copper ions in environmental water samples. Environ Monit Assess 187:601–610

Skoczko I, Szatyłowicz E (2018) Removal of heavy metal ions by filtration on activated alumina-assisted magnetic field. Desalin Water Treat 117:345–352

Süreyya M, Guida M, Anselmo A, Mattei ML, Pagano G (2002) Microbial and cod removal in a municipal wastewater treatment plant using coagulation flocculation process. Envion Lett 37:1483–1494

Tripathy S, Bhandari V, Sharma P, Vanjari SRK, Singh SG (2019) Chemiresistive DNA hybridization sensor with electrospun nanofibers: a method to minimize inter-device variability. Biosens Bioelectron 133:24–31

Wang B, Bai Z, Jiang H, Prinsen P, Luque R, Zhao S, Jin X (2019a) Selective heavy metal removal and water purification by microfluidically-generated chitosan microspheres: characteristics, modeling and application. J Hazard Mater 364:192–205

Wang L, Li J, Wang J, Guo X, Wang X, Choo J, Chen L (2019b) Green multi-functional monomer based ion imprinted polymers for selective removal of copper ions from aqueous solution. J Colloid Interface Sci 541:376–386

Wu GH, Song GC, Wu DY, Shen YY, Wang ZQ, He CY (2010) Synthesis of ion-imprinted mesoporous silica gel sorbent for selective adsorption of copper ions in aqueous media. Microchim Acta 171:203–209

Wu RX, Zheng GF, Li WW, Zhong LB, Zheng YM (2018) Electrospun chitosan nanofiber membrane for adsorption of Cu(II) from aqueous solution: fabrication, characterization and performance. J Nanosci Nanotechnol 18:5624–5635

Xu J, Cao Z, Zhang Y, Yuan Z, Lou Z, Xu X, Wang X (2018a) A review of functionalized carbon nanotubes and graphene for heavy metal adsorption from water: preparation, application, and mechanism. Chemsophere 195:351–364

Xu J, Chen Y, Zheng L, Liu B, Liu J, Wang X (2018b) Assessment of heavy metal pollution in the sediment of the main tributaries of dongting lake, China. Water 10:1060

Yu H, Chen X, Cai J, Ye D, Wu Y, Liu P (2018) Dual controlled release nanomicelle-in-nanofiber system for long-term antibacterial medical dressings. J Biomat Sci Polym E 30:1–25

Zhang N, Hu B, Huang C (2007) A new ion-imprinted silica gel sorbent for on-line selective solid-phase extraction of dysprosium(III) with detection by inductively coupled plasma-atomic emission spectrometry. Anal Chim Acta 597:12–18

Zhang Z, Xu X, Yan Y (2010) Kinetic and thermodynamic analysis of selective adsorption of Cs(I) by a novel surface whisker-supported ion-imprinted polymer. Desalination 263:97–106

Zhang S, Shi Q, Christodoulatos C, Korfiatis G, Meng X (2019) Adsorptive filtration of lead by electrospun PVA/PAA nanofiber membranes in a fixed-bed column. Chem Eng J 370:1262–1273

Zhao B, Jiang H, Lin Z, Xu S, Zhang A (2019) Preparation of acrylamide/acrylic acid cellulose hydrogels for the adsorption of heavy metal ions. Carbohydr Polym 224:115022

Zhijiang C, Ping X, Shiqi H, Cong Z (2019) Soy protein nanoparticles modified bacterial cellulose electrospun nanofiber membrane scaffold by ultrasound-induced self-assembly technique: characterization and cytocompatibility. Cellulose 26:6133–6150

Zhu H, Jia S, Wan T, Jia Y, Yang H, Li J, Cheng Z (2011) Biosynthesis of spherical Fe_3O_4/bacterial cellulose nanocomposites as adsorbents for heavy metal ions. Carbohydr Polym 86:1558–1564

Zhu Y, Bai ZS, Wang HL (2017) Microfluidic synthesis of thiourea modified chitosan microsphere of high specific surface area for heavy metal wastewater treatment. Chinese Chem Lett 28:633–641